# The Liverwort, *Marchantia*, Drives Alternative Electron Flow Using a Flavodiiron Protein to Protect PSI[1][OPEN]

**Ginga Shimakawa[2], Kimitsune Ishizaki[2], Shigeyuki Tsukamoto, Moeko Tanaka, Takehiro Sejima, and Chikahiro Miyake***

Graduate School of Agricultural Science (G.S., M.T., T.S., C.M.) and Graduate School of Science (K.I., S.T.), Kobe University, Nada, Kobe 657-8501, Japan; and Core Research for Environmental Science and Technology, Japan Science and Technology Agency, Chiyoda-ku, Tokyo 102-0076, Japan (C.M.)

**ORCID IDs: 0000-0002-8557-2096 (G.S.); 0000-0003-0504-8196 (K.I.); 0000-0002-5318-3707 (M.T.); 0000-0002-2426-2377 (C.M.).**

The diffusion efficiency of oxygen in the atmosphere, like that of $CO_2$, is approximately $10^4$ times greater than that in aqueous environments. Consequently, terrestrial photosynthetic organisms need mechanisms to protect against potential oxidative damage. The liverwort *Marchantia polymorpha*, a basal land plant, has habitats where it is exposed to both water and the atmosphere. Furthermore, like cyanobacteria, *M. polymorpha* has genes encoding flavodiiron proteins (FLV). In cyanobacteria, FLVs mediate oxygen-dependent alternative electron flow (AEF) to suppress the production of reactive oxygen species. Here, we investigated whether FLVs are required for the protection of photosynthesis in *M. polymorpha*. A mutant deficient in the FLV1 isozyme (Δ*MpFlv1*) sustained photooxidative damage to photosystem I (PSI) following repetitive short-saturation pulses of light. Compared with the wild type (Takaragaike-1), Δ*MpFlv1* showed the same photosynthetic oxygen evolution rate but a lower electron transport rate during the induction phase of photosynthesis. Additionally, the reaction center chlorophyll in PSI, P700, was highly reduced in Δ*MpFlv1* but not in Takaragaike-1. These results indicate that the gene product of *MpFlv1* drives AEF to oxidize PSI, as in cyanobacteria. Furthermore, FLV-mediated AEF supports the production of a proton motive force to possibly induce the nonphotochemical quenching of chlorophyll fluorescence and suppress electron transport in the cytochrome $b_6/f$ complex. After submerging the thalli, a decrease in photosystem II operating efficiency was observed, particularly in Δ*MpFlv1*, which implies that species living in these sorts of habitats require FLV-mediated AEF.

A decrease in the efficiency of light usage for photosynthetic $CO_2$ fixation in the Calvin-Benson cycle enhances the likelihood that oxygenic phototrophs will suffer from photooxidative damage caused by reactive oxygen species (ROS; Miyake, 2010). For example, under conditions of high light, low $CO_2$, and/or low temperature, the light energy absorbed by PSI and PSII in thylakoid membranes exceeds requirements, because turnover of the Calvin-Benson cycle limits the regeneration of $NADP^+$. Consequently, electrons accumulate in the photosynthetic electron transport (PET) system. The accumulated electrons start to flow to oxygen, producing ROS, including superoxide anion radicals and hydrogen peroxide, in PSI (Krieger-Liszkay, 2005; Sejima et al., 2014; Zivcak et al., 2015a, 2015b; Takagi et al., 2016). Furthermore, the accumulation of electrons in the PET system suppresses the charge separation of the reaction center chlorophylls (Chls), P680 in PSII and P700 in PSI, which stimulates the production of another ROS, singlet oxygen (Cazzaniga et al., 2012; Fischer et al., 2013). It is proposed that the reduced state of P700 in PSI under illuminated conditions stimulates the production of singlet oxygen and superoxide anion radicals to inactivate PSI, resulting in a decline in photosynthetic $CO_2$ fixation (Cazzaniga et al., 2012; Rutherford et al., 2012; Sejima et al., 2014; Zivcak et al., 2015a, 2015b; Takagi et al., 2016).

Oxygenic phototrophs have various systems that can be used to suppress electron accumulation in the PET system; they are broadly divided into two groups. The first group uses regulation of the absorption efficiency of photon energy into the PET system, which includes nonphotochemical quenching (NPQ) of Chl fluorescence and state transition (Derks et al., 2015). In the second group, electron sinks consume excess photon energy as futile electron pathways with heat dissipation. These

[1] This work was supported by the Japan Society for the Promotion of Science (grant no. 26450079 to C.M. and grant no. 16J03443 to G.S.) and by the Core Research for Evolutional Science and Technology division of the Japan Science and Technology Agency (grant no. AL65D21010 to C.M.).

[2] These authors contributed equally to the article.

* Address correspondence to cmiyake@hawk.kobe-u.ac.jp.

The author responsible for distribution of materials integral to the findings presented in this article in accordance with the policy described in the Instructions for Authors (www.plantphysiol.org) is: Chikahiro Miyake (cmiyake@hawk.kobe-u.ac.jp).

C.M. conceived the original screening and research plans; C.M. and K.I. supervised the experiments; G.S. performed most of the experiments; K.I., S.T., M.T., and T.S. provided technical assistance to G.S.; C.M. and G.S. designed the experiments and analyzed the data; C.M. and G.S. conceived the project and wrote the article with contributions from all the authors; C.M. supervised and complemented the writing.

[OPEN] Articles can be viewed without a subscription.

www.plantphysiol.org/cgi/doi/10.1104/pp.16.01038

 

electron sinks constitute alternative electron flow (AEF), and the representatives are observed as photorespiration and Mehler-like reactions (Kozaki and Takeba, 1996; Asada, 1999; Helman et al., 2003; Takahashi et al., 2007; Hayashi et al., 2014; Shimakawa et al., 2015; Sejima et al., 2016).

With regard to the protection of PSI against photooxidative damage, there is a further strategy in addition to NPQ and AEF that suppresses photosynthetic electron transport in the cytochrome $b_6/f$ complex in the center of the PET system. This suppression is triggered by the integration of a proton gradient across thylakoid membranes (ΔpH; Kramer et al., 1999) or the reduction of the plastoquinone (PQ) pool (Shaku et al., 2016), which contributes to the oxidation of PSI. Furthermore, ΔpH also is involved in the induction of the molecular mechanisms of some NPQ (Derks et al., 2015). Collectively, oxygenic phototrophs harbor many systems for the alleviation of photooxidative damage that are rich in diversity and have been acquired or lost by species over their evolutionary history.

One of the most enduring mysteries is whether a molecular mechanism of AEF has been lost over the long history of evolutionary processes in oxygenic phototrophs. In the progenitor cyanobacteria, Helman et al. (2003) found a large AEF to oxygen, which is not photorespiration, and showed that the AEF is driven by FLAVODIIRON PROTEIN1 (FLV1) and FLV3. Some cyanobacteria have four isozymes of FLV (FLV1−FLV4), whereas others have just two: FLV1 and FLV3. FLV1/3 and FLV2/4 function as heterodimers (Zhang et al., 2012; Allahverdiyeva et al., 2013). In *Synechocystis* sp. PCC 6803 (S. 6803), both FLV1/3 and FLV2/4 mediate oxygen-dependent AEF as well as oxidize the PET system under $CO_2$-saturated and $CO_2$-limited conditions, respectively (Helman et al., 2003; Hayashi et al., 2014; Shimakawa et al., 2015). An S. 6803 mutant deficient in FLV1/3 was shown to sustain oxidative damage under fluctuating light (Allahverdiyeva et al., 2013), and another mutant deficient in FLV2/4 also suffered under low-$CO_2$ conditions (Zhang et al., 2012). These data indicate that FLV is essential for the alleviation of photooxidative damage in cyanobacteria. Surprisingly, during the course of evolution, the isozymes of FLV have been lost in seed plants at the gene level (Yamamoto et al., 2016). On the basis of accumulated genomic information, FLV1/3 isozymes are found to be broadly conserved in the photosynthetic green plant lineage, including cyanobacteria, green algae, bryophytes, pteridophytes, and pinophytes; there is more sequence variation between basal land plants and cyanobacteria than there is among cyanobacteria (Yamamoto et al., 2016). This suggests that, at some point in the course of evolution, oxygenic phototrophs no longer had a need for FLV. However, the physiological functions of FLV in phototrophs other than cyanobacteria have yet to be elucidated.

The liverwort *Marchantia polymorpha* is positioned between algae and plants in the photosynthetic green plant lineage (Bowman et al., 2007) and has two genes encoding isozymes of FLV1/3 (*MpFlv1* [*Mapoly0005s0210*] and *MpFLV3* [*Mapoly0103s0039*]). Additionally, one of the habitats of *M. polymorpha* is the marginal area between aquatic and land environments; thus, this plant sometimes experiences both submergence and drought stress. Submergence limits the diffusion of gases. The diffusion coefficient of $CO_2$ in water is approximately $10^{-4}$ times lower than that in the atmosphere, which depresses photosynthetic $CO_2$ fixation (Raven et al., 1985; Badger and Spalding, 2000). Furthermore, another habitat of the liverwort is the forest floor, where photon energy from the sun is provided as fluctuating light termed sunfleck (Boardman, 1977). These habitat situations suggest that *M. polymorpha* would require sufficient AEF activity to escape from oxidative damage through the dissipation of excess photon energy.

In this study, we sought to clarify the physiological functions of FLV in *M. polymorpha* by comparing the wild type (Takaragaike-1 [Tak-1]) and a mutant deficient in *MpFlv1* (Δ*MpFlv1*). We found that the activity of AEF was mediated by FLV, which supports the formation of ΔpH that contributes to the protection of PSI against photooxidative damage under the fluctuating light conditions in which *M. polymorpha* grows.

## RESULTS AND DISCUSSION

### Effects of FLV on Photooxidative Damage to PSI in *M. polymorpha*

We constructed the mutant Δ*MpFlv1* through targeted disruption of the gene *MpFlv1* (Supplemental Fig. S1). We found that the maximum quantum efficiency of PSII photochemistry ($F_v/F_m$) in Δ*MpFlv1* was not different from that of the wild-type Tak-1 or of the complement mutant to Δ*MpFlv1* (c*MpFlv1*; Table I). Additionally, total amounts of Chl *a* and *b* were almost the same among these plants (Table I). Furthermore, the total nitrogen content of Δ*MpFlv1* also was at the same level as those in Tak-1 and c*MpFlv1* (Table I). These data indicate that the deletion of *MpFlv1* has little effect on the growth of *M. polymorpha* under the growth conditions used in this study.

To investigate the physiological functions of FLV in the protection of PSI and PSII in *M. polymorpha*, we illuminated the thalli of Tak-1, Δ*MpFlv1*, and c*MpFlv1* with short-saturation pulses. Repetitive short-saturation pulse (rSP) illumination saturates the PET system with electrons to selectively inactivate PSI, with oxygen required in $C_3$ plant leaves (Sejima et al., 2014; Zivcak et al., 2015a, 2015b). In sunflower (*Helianthus annuus*) leaves, total oxidizable P700 ($P_m$) decreased to about 10% of the initial value through rSP treatment (300 ms, 20,000 $\mu$mol photons $m^{-2}$ $s^{-1}$, every 10 s) for 4 h, whereas $F_v/F_m$ decreased to about 80% (Sejima et al., 2014). Hence, rSP treatment is a useful method of inducing the photoinhibition of PSI in vivo and of investigating the robustness of PSI against photooxidative damage.

In Δ*MpFlv1*, rSP treatment (1 s, 3,000 $\mu$mol photons $m^{-2}$ $s^{-1}$, every 10 s) significantly decreased both

**Table I.** *Characteristics of Tak-1, ΔMpFlv1, and cMpFlv1*

Data are shown as means ± SD of three independent measurements.

| Plant | $F_v/F_m$ | Total Chl | Chl *a*/Chl *b* | Total Nitrogen |
|---|---|---|---|---|
| | | $g\ m^{-2}$ | | $g\ m^{-2}$ |
| Tak-1 | 0.811 ± 0.008 | 0.20 ± 0.03 | 2.97 ± 0.12 | 0.79 ± 0.12 |
| Δ*MpFlv1* | 0.804 ± 0.004 | 0.20 ± 0.01 | 3.08 ± 0.04 | 0.76 ± 0.06 |
| c*MpFlv1* | 0.803 ± 0.018 | 0.22 ± 0.04 | 3.03 ± 0.08 | 0.73 ± 0.11 |

$P_m$ and $F_v/F_m$, as compared with its effect in Tak-1 (Fig. 1), which suggests that photoinhibition of PSI and PSII occurs during rSP treatment in Δ*MpFlv1*. Posttreatment $P_m$ and $F_v/F_m$ were measured after a 30-min incubation in the dark to relax the influence of NPQ, state transition, and chloroplast movements. Complementation of Δ*MpFlv1* with *MpFlv1* partially relieved the photoinhibition of both PSI and PSII (Fig. 1). In Δ*MpFlv1*, the degree of decrease in $P_m$ was greater than that in $F_v/F_m$ (Fig. 1), indicating that, in liverworts as in $C_3$ plants, rSP treatment leads to photooxidative damage mainly in PSI (Sejima et al., 2014; Zivcak et al., 2015a, 2015b). Compared with rSP treatment in air, the extent of PSI damage was smaller in Δ*MpFlv1* during treatment in the absence of oxygen (Fig. 1A), which suggests that the photoinhibition of PSI in Δ*MpFlv1* is caused by ROS. In contrast, the decrease in $F_v/F_m$ during rSP treatment was accelerated in the absence of oxygen (Fig. 1B). In PSII, oxygen-insensitive photodamage might occur during rSP treatment (Krause et al., 1985).

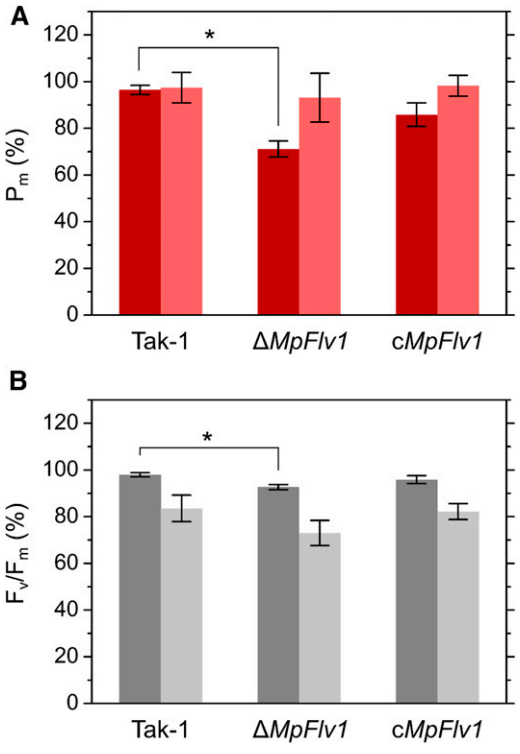


**Figure 1.** Effects of rSP treatment on $P_m$ (A) and $F_v/F_m$ (B) in Tak-1, Δ*MpFlv1*, and c*MpFlv1* in ambient air (dark-colored bars) and pure $N_2$ gas (light-colored bars). These values were obtained 30 min (in the dark) after 15-min treatments. For rSP treatments, rSPs (3,000 μmol photons $m^{-2}\ s^{-1}$, 1 s) were applied every 10 s in the dark. Data are represented as means ± SD of six independent measurements. Differences between Tak-1 and Δ*MpFlv1* were analyzed using Student's *t* test. Asterisks indicate statistically significant differences between Tak-1 and Δ*MpFlv1* at $P < 0.05$.

### Effects of FLV on Photosynthesis in *M. polymorpha*

As shown in Figure 1A, FLV is required to protect PSI against photooxidative damage, which implies that the functions of FLV-mediated AEF in *M. polymorpha* are similar to those in cyanobacteria. To test this hypothesis, we simultaneously monitored oxygen exchange and the quantum yield of photochemical energy conversion in PSII (PSII operating efficiency), Y(II), in Tak-1, Δ*MpFlv1*, and c*MpFlv1* (Fig. 2). Before illumination with actinic light (AL), we determined dark respiration rates to be 1.5 ± 0.5, 1.7 ± 0.7, and 1.6 ± 0.5 μmol oxygen $m^{-2}\ s^{-1}$ in the thalli of Tak-1, Δ*MpFlv1*, and c*MpFlv1*, respectively ($n = 6$). Upon illumination of the thalli, gross photosynthetic oxygen evolution rates (net oxygen evolution rate + dark respiration rate) increased gradually during photosynthetic induction. Similar to Tak-1, Δ*MpFlv1* showed an induction of photosynthesis (Fig. 2A). Furthermore, c*MpFlv1* also showed the same rate of photosynthetic induction as Tak-1 and Δ*MpFlv1*. That is, the deficiency of *MpFlv1* did not affect photosynthesis. However, the behavior of Y(II) in these plants differed in the oxygen evolution rate during the induction of photosynthesis. In Tak-1, Y(II) started to increase before the increase in the oxygen evolution rate, just after the commencement of illumination (Fig. 2B). In contrast, in Δ*MpFlv1*, the increase in Y(II) was delayed and started to increase at 1 min after illumination was started. Y(II) in c*MpFlv1*, however, showed the same behavior as in Tak-1. These data indicate that, in *M. polymorpha*, the gene product of *MpFlv1* functions in AEF before the start of steady-state photosynthesis, which also is observed in the cyanobacterium S. 6803 (Supplemental Fig. S2). Both gross photosynthetic oxygen evolution rate and Y(II) in Δ*MpFlv1* reached the same values as those in Tak-1 and c*MpFlv1* at steady-state photosynthesis (Fig. 2). We evaluated the dependence of the gross photosynthetic oxygen evolution rate and Y(II) on photon flux density in Tak-1, Δ*MpFlv1*, and c*MpFlv1* (Supplemental Fig. S3). These data suggest that the effect of FLV on photosynthesis is smaller at steady state compared with the induction phase.

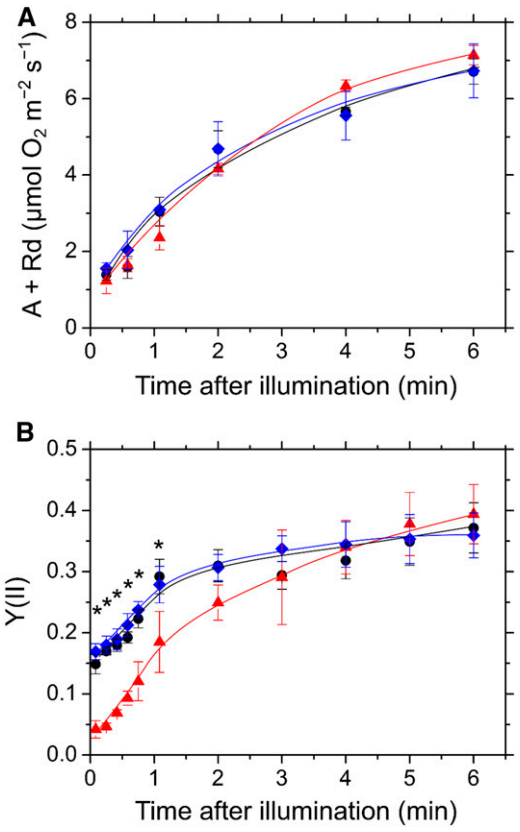


**Figure 2.** Time course of gross photosynthetic oxygen evolution rate (A; A) and Y(II) (B) in the induction phase of photosynthesis in Tak-1 (black circles), Δ*MpFlv1* (red triangles), and c*MpFlv1* (blue diamonds). Rd, Dark respiration rate. $CO_2$-saturated conditions were generated by adding 1 M $NaHCO_3$ to the felt mat in the reaction chamber. AL (200 μmol photons $m^{-2}$ $s^{-1}$) was turned on at the zero time point. Data are represented as means ± SD of three independent measurements. Differences in Y(II) between Tak-1 and Δ*MpFlv1* were analyzed using Student's *t* test. Asterisks indicate statistically significant differences between Tak-1 and Δ*MpFlv1* at $P < 0.05$.

### Effects of FLV on Photosynthetic Parameters in PSII and PSI in *M. polymorpha*

In *M. polymorpha*, the gene product of *MpFlv1* mediates AEF (Fig. 2), and its absence accelerates photooxidative damage to PSI (Fig. 1A). In plant leaves and cyanobacterial cells, photoinhibition of PSI is alleviated by the oxidation of P700, owing to a decrease in the amount of photooxidizable P700 (Sejima et al., 2014; Shimakawa et al., 2016b). These data indicate that FLV-mediated AEF contributes to the oxidation of P700 in *M. polymorpha*. To clarify the effects of FLV on the PET system in *M. polymorpha*, we investigated photosynthetic parameters in PSII and PSI in Tak-1, Δ*MpFlv1*, and c*MpFlv1* in the response to illumination with AL.

First, we examined the photosynthetic parameters in PSII using Chl fluorescence measurement. In both Tak-1 and c*MpFlv1*, Y(II) was higher than that in Δ*MpFlv1* during the induction phase of photosynthesis (Fig. 3A). Thereafter, the Y(II) in Δ*MpFlv1* became more similar to those in Tak-1 and c*MpFlv1* with photosynthesis induction (Fig. 3A). Additionally, compared with Δ*MpFlv1*, the observed NPQ also was higher in Tak-1 and c*MpFlv1* in response to illumination with AL (Fig. 3B). Furthermore, the coefficient of photochemical quenching of Chl fluorescence (qP) was higher in Tak-1 and c*MpFlv1* than in Δ*MpFlv1* (Fig. 3C). The light-response curves of Y(II), NPQ, and qP during steady-state photosynthesis also are shown (Fig. 4, A–C). Similar to Y(II), NPQ and qP had almost the same values at steady-state photosynthesis in these three plants, with the exception of illumination with high light leading to lower Y(II), NPQ, and qP in Δ*MpFlv1* than in Tak-1 and c*MpFlv1* (Fig. 4, A–C). Some of the discrepancy between Y(II) values depicted in Figure 4A and Supplemental Figure S3B might be due to differences in the equipment used to measure Chl fluorescence. Thus, we can draw the following tentative conclusions from the foregoing results. FLV drives photosynthetic linear electron flow as AEF, which would induce ΔpH to trigger NPQ (Derks et al., 2015). Both the stimulated electron sink and the enhanced NPQ caused by FLV-mediated AEF contribute to oxidation of the PET system, as demonstrated by the increase in qP (Figs. 3C and 4C; Miyake, 2008).

Next, we investigated the effects of FLV on the photosynthetic parameters in PSI, evaluated by examining changes in the absorbance of P700 (Klughammer and Schreiber, 1994; Schreiber and Klughammer, 2008). Similar to Y(II), we found higher quantum yields of PSI, Y(I), in Tak-1 and c*MpFlv1* than in Δ*MpFlv1* (Fig. 3D). We note that we cannot exclude the possibility that the deletion of FLV affects the distribution of PSII and PSI. Additionally, we measured the redox state of P700 in the induction phase of photosynthesis. Both Tak-1 and c*MpFlv1* showed larger donor-side limitation of PSI, Y(ND), than Δ*MpFlv1* (Fig. 3E), indicating that FLV-mediated AEF causes the Y(ND). In contrast, the acceptor-side limitations of PSI, Y(NA), were lower in Tak-1 and c*MpFlv1* than in Δ*MpFlv1* (Fig. 3F). That is, deletion of *MpFlv1* changed the limiting step from the donor side to the acceptor side of PSI. Thus, FLV contributes to the oxidation of P700 in the induction phase of photosynthesis in *M. polymorpha*, which might be responsible for the protection of PSI against photoinhibition (Fig. 1A). In c*MpFlv1*, lower Y(ND) and higher Y(NA) than those in Tak-1 were observed just after starting illumination (Fig. 3, E and F). The reason for this difference is unclear, but the recombinant gene product of *MpFlv1* in c*MpFlv1* might not function as well as the gene product expressed in Tak-1. The amount of the recombinant protein present in c*MpFlv1* also should be considered. The photosynthetic parameters, including Y(I), Y(ND), and Y(NA), in Δ*MpFlv1* changed in a time-dependent manner to reach almost the same values as those in Tak-1 and c*MpFlv1* at steady-state photosynthesis (Fig. 3, D–F). The light-response curves of Y(I), Y(ND), and Y(NA) during steady-state photosynthesis suggest that the contribution of FLV-mediated AEF to regulating the

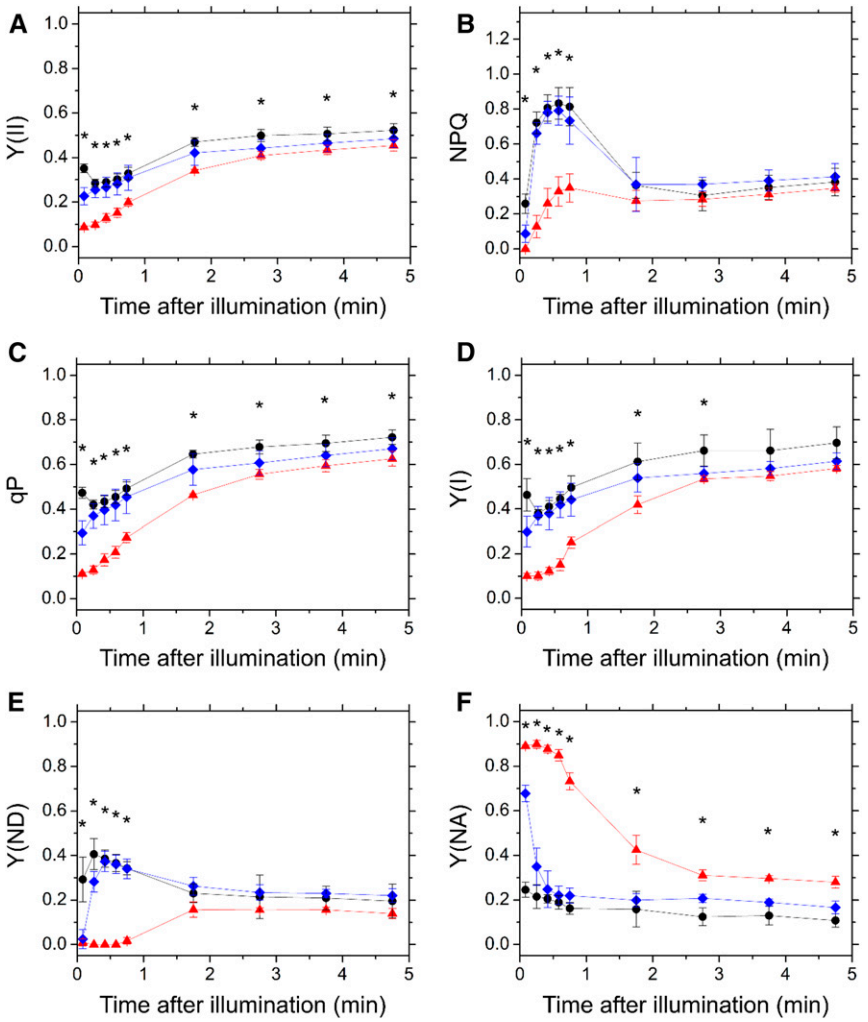


**Figure 3.** Time course of Y(II) (A), NPQ (B), qP (C), Y(I) (D), Y(ND) (E), and Y(NA) (F) in the induction phase of photosynthesis in Tak-1 (black circles), Δ*MpFlv1* (red triangles), and c*MpFlv1* (blue diamonds). AL (195 $\mu$mol photons $m^{-2}$ $s^{-1}$) was turned on at the zero time point. Measurements were taken in ambient air. Data are represented as means ± SD of three independent measurements. Differences between Tak-1 and Δ*MpFlv1* were analyzed using Student's *t* test. Asterisks indicate statistically significant differences between Tak-1 and Δ*MpFlv1* at $P < 0.05$.

redox state of PSI is smaller at steady-state photosynthesis, compared with the induction phase, although significant differences were found between Tak-1 and Δ*MpFlv1* under high light (Fig. 4, D–F).

Furthermore, we measured photosynthetic parameters in PSII and PSI under a fluctuating light condition in Tak-1, Δ*MpFlv1*, and c*MpFlv1*. The thalli of these plants were illuminated with AL (200 $\mu$mol photons $m^{-2}$ $s^{-1}$) to reach steady-state photosynthesis, and then we increased the photon flux density of AL by approximately 4-fold (840 $\mu$mol photons $m^{-2}$ $s^{-1}$). During the transition from moderate to high light, Chl fluorescence and P700 absorbance were monitored simultaneously.

Both Y(II) and qP decreased in response to the transition to high light in all strains, with the largest decrease being observed in Δ*MpFlv1* (Fig. 5, A and C). Thereafter, lowered Y(II) and qP in Δ*MpFlv1* increased gradually to reach constant values approximately 4 min after the change in photon flux density, although both Y(II) and qP were initially maintained at constant levels in Tak-1 and c*MpFlv1* after the transition (Fig. 5, A and C). Additionally, the induction of NPQ by illumination with high light was retarded significantly in Δ*MpFlv1* compared with its induction in the other strains (Fig. 5B). The behaviors of these photosynthetic parameters in PSII were consistent with those in photosynthesis induction (Fig. 3, A–C).

In the case of PSI, the decrease in Y(I) during the transition from moderate to high light was largest in Δ*MpFlv1* (Fig. 5D), similar to the responses of Y(II) and qP (Fig. 5, A and C). In both Tak-1 and c*MpFlv1*, Y(ND) rose rapidly in response to high light and then decreased gradually to a constant level (Fig. 5E). However, Δ*MpFlv1* showed a slower induction of Y(ND) than was observed in Tak-1 and c*MpFlv1* (Fig. 5E). In contrast, a rapid increase in Y(NA) was observed in Δ*MpFlv1* during the transition to high light, whereas in Tak-1 and c*MpFlv1*, Y(NA) was not affected by the change in photon flux density (Fig. 5F). These data suggest that FLV-mediated AEF is required to maintain P700 in an oxidized state under fluctuating light in *M. polymorpha*, which is similar to observations of the cyanobacterium S. 6803 (Allahverdiyeva et al., 2013; Shimakawa et al., 2016b).

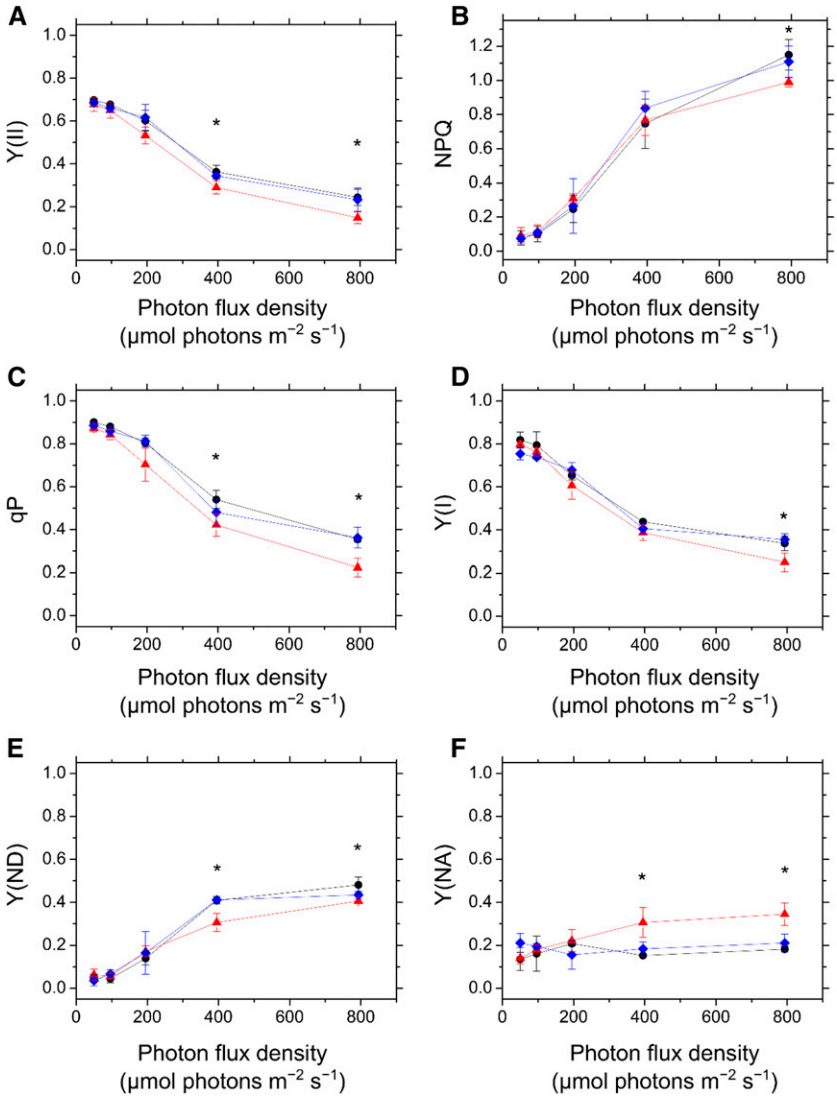


**Figure 4.** Dependence of Y(II) (A), NPQ (B), qP (C), Y(I) (D), Y(ND) (E), and Y(NA) (F) on photon flux density at steady-state photosynthesis in Tak-1 (black circles), Δ*MpFlv1* (red triangles), and c*MpFlv1* (blue diamonds). Measurements were taken in ambient air. Data are represented as means ± SD of three independent measurements. Differences between Tak-1 and Δ*MpFlv1* were analyzed using Student's *t* test. Asterisks indicate statistically significant differences between Tak-1 and Δ*MpFlv1* at $P < 0.05$.

### Effects of FLV on Thylakoid Membrane Potential in *M. polymorpha*

To clarify the relationship between the FLV-mediated AEF and P700 oxidation, we evaluated the effects of FLV on thylakoid membrane potential in *M. polymorpha* by analyzing electrochromic shift (ECS, or P515, because the absorption measurements are made at 515 nm) signals (Klughammer et al., 2013) in the response to high light in Tak-1, Δ*MpFlv1*, and c*MpFlv1*. The ECS signal is considered an intrinsic optical voltmeter that responds rapidly to changes in the electrical potential across the thylakoid membrane (Witt, 1979) and can be utilized in a noninvasive spectroscopic measurement (Baker et al., 2007; Bailleul et al., 2010; Klughammer et al., 2013; Johnson and Ruban, 2014). The thylakoid membrane potential during photosynthesis is defined as the total rapid (less than 1 s) change in the ECS signal (ECSt) upon rapidly switching off AL from steady state, which reflects the light-dark difference in proton motive force, and includes two components: transmembrane differences in the concentration of protons (ΔpH) and in the electric field ($\Delta\Psi$; Sacksteder and Kramer, 2000; Cruz et al., 2001, 2005; Baker et al., 2007). In this study, the values of ECSt were normalized by dividing the magnitude of ECS decay in dark-interval relaxation kinetics (DIRK) analysis by the magnitude of ECS induced by a 10-$\mu$s single-turnover flash (Klughammer et al., 2013). The initial decay rate of the ECS signal following light-to-dark transitions can be used to estimate relative light-driven proton flux through the chloroplast ATP synthase ($H^+$ efflux rate [$v_H^+$]), which is known to have a linear relationship with the photosynthetic linear electron transport rate only if there is no contribution to proton flux from cyclic electron flow around PSI (Avenson et al., 2005). Furthermore, the first-order decay time of the ECS decay in the light-to-dark transitions is required for the estimation of proton conductance in ATP synthase ($g_H^+$; Kanazawa and Kramer, 2002). We note that the ECS parameters are dependent on the properties of the leaves, not only the

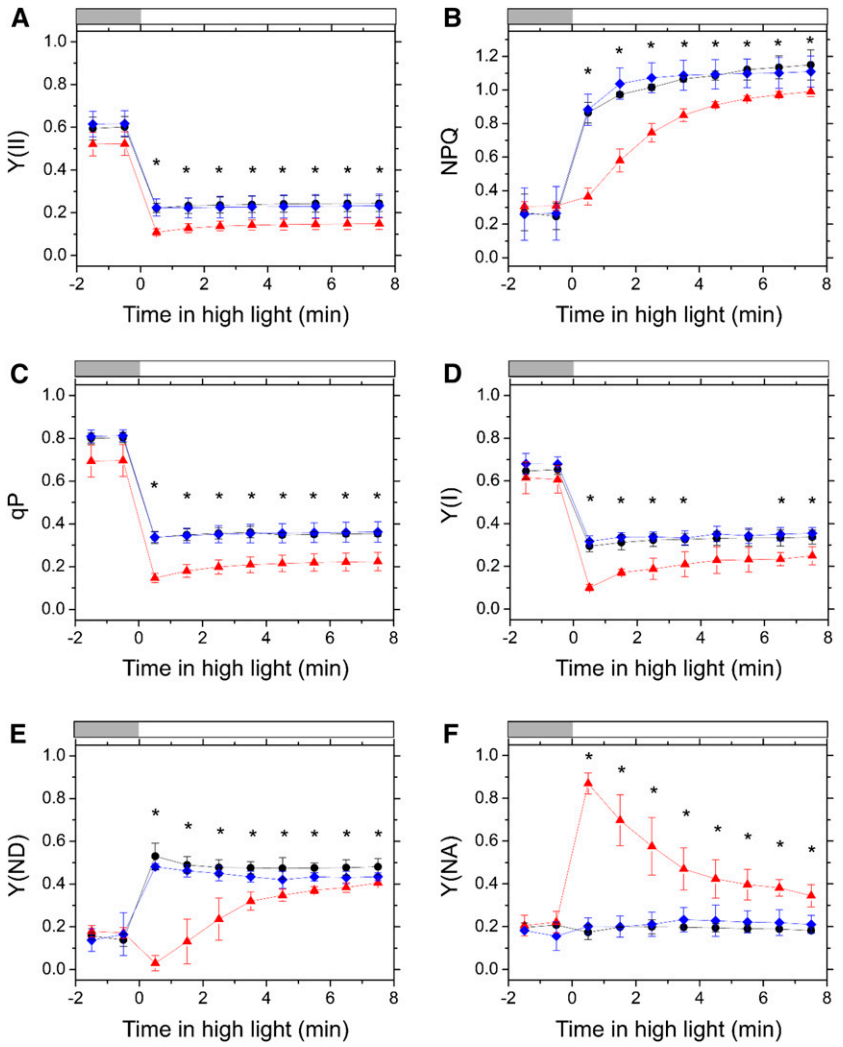


**Figure 5.** Time course of Y(II) (A), NPQ (B), qP (C), Y(I) (D), Y(ND) (E), and Y(NA) (F) in the transition from moderate light (200 $\mu$mol photons $m^{-2}$ $s^{-1}$; light gray bars) to high light (840 $\mu$mol photons $m^{-2}$ $s^{-1}$; white bars) in Tak-1 (black circles), Δ*MpFlv1* (red triangles), and c*MpFlv1* (blue diamonds). Measurements were taken in ambient air. Data are represented as means ± SD of three independent measurements. Differences between Tak-1 and Δ*MpFlv1* were analyzed using Student's *t* test. Asterisks indicate statistically significant differences between Tak-1 and Δ*MpFlv1* at $P < 0.05$.

density of chloroplasts but also the content of light-harvesting complexes that house the shifted pigments.

A lack of FLV had some impact on the ECS parameters during the transition to high light in *M. polymorpha*. The representative original kinetics of the ECS signal following light-to-dark transitions in Tak-1 and Δ*MpFlv1* are shown in Supplemental Figure S4 and were utilized to estimate the ECS parameters of the following results. In response to high light, ECSt in Tak-1 and c*MpFlv1* first increased rapidly and thereafter decreased gradually (Fig. 6A; Supplemental Fig. S5A). Compared with Tak-1 and c*MpFlv1*, ECSt in Δ*MpFlv1* decreased just after the start of illumination with high light, which was accompanied by an increase in $g_H^+$, and thereafter increased gradually (Fig. 6A; Supplemental Fig. S5, A and B). We divided ECSt into ΔpH and ΔΨ following the method described by Klughammer et al. (2013), indicating that, in *M. polymorpha*, FLV-mediated AEF stimulates photosynthetic linear electron flow to support the establishment of ΔpH (Fig. 6). It is still unclear why $g_H^+$ increased in Δ*MpFlv1* just after the thalli were exposed to high light (Supplemental Fig. S5B). In contrast, $V_H^+$ increased slightly in response to high light in all three of the plants (Supplemental Fig. S5C).

We evaluated the dependence of the relative electron transport rate at PSII (rETR), calculated as the product of Y(II) and photon flux density, and ECS parameters on photon flux density during steady-state photosynthesis in Tak-1, Δ*MpFlv1*, and c*MpFlv1* (Supplemental Figs. S6 and S7), which shows the increase in rETR uncoupled with ECSt in the range of photon flux density approximately over 200 $\mu$mol photons $m^{-2}$ $s^{-1}$. Unfortunately, we could not determine the reasons for the gap between ECSt and rETR in *M. polymorpha*. In intact chloroplasts and plant leaves, cyclic electron flow within PSII drives to oxidize the PQ pool, which is sensitive to ΔpH (Miyake and Yokota, 2001; Miyake et al., 2002; Miyake and Okamura, 2003; Laisk et al., 2006). In *M. polymorpha*, FLV-mediated AEF might function in the induction of cyclic electron flow within PSII through the formation of ΔpH, resulting in the increases in Y(II) and qP (Fig. 4C; Supplemental Figs. S6, A and B, and S7, A–D). The other possibility is that changes in the ratio between components of the

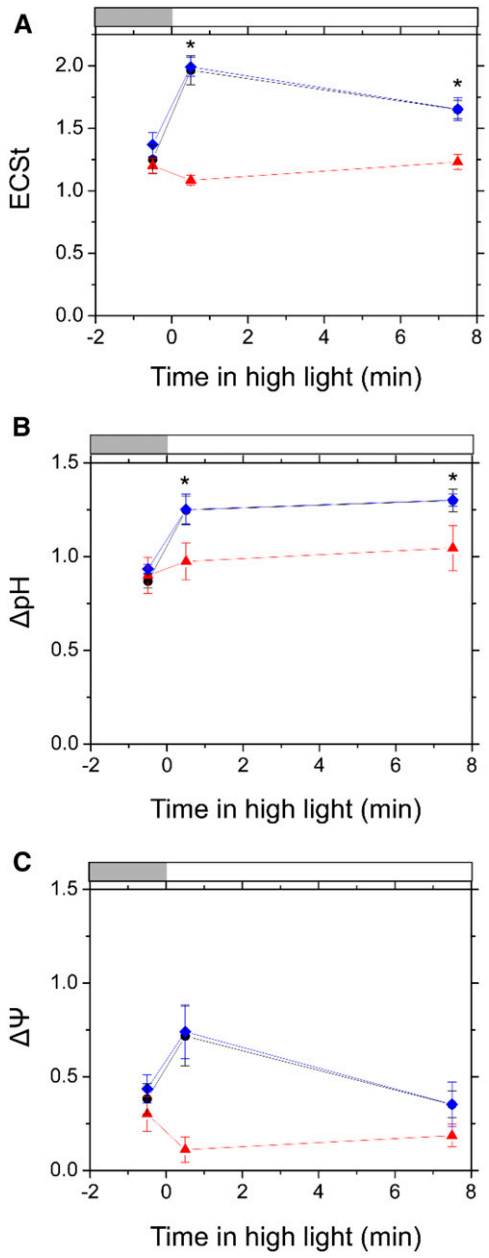


**Figure 6.** Time course of ECSt (A), ΔpH (B), and ΔΨ (C) during the transition from moderate light (200 $\mu$mol photons $m^{-2}$ $s^{-1}$; light gray bars) to high light (830 $\mu$mol photons $m^{-2}$ $s^{-1}$; white bars) in Tak-1 (black circles), Δ*MpFlv1* (red triangles), and c*MpFlv1* (blue diamonds). Measurements were taken in ambient air. Data are represented as means ± SD of three independent measurements. Differences between Tak-1 and Δ*MpFlv1* were analyzed using Student's *t* test. Asterisks indicate statistically significant differences between Tak-1 and Δ*MpFlv1* at $P < 0.05$.

photosynthetic machinery, including state transition, might be related to these results.

We also evaluated the relationship of NPQ with rETR during steady-state photosynthesis in Tak-1, Δ*MpFlv1*, and c*MpFlv1*. In plant leaves, NPQ is observed mainly in the form of energy-dependent quenching (qE), which is proportional to ΔpH but not to ΔΨ, and involves a fast (seconds to a few minutes time scale) PSII antenna reorganization (Avenson et al., 2004; Takizawa et al., 2007; Derks et al., 2015). Nevertheless, NPQ did not show the linear relationship with rETR in all three strains of *M. polymorpha* (Supplemental Fig. S8) in the range of rETR that was proportional to ΔpH (Supplemental Fig. S7D). We measured the time scale of the relaxation of NPQ after turning off AL in Tak-1 (Supplemental Fig. S9), which suggests that ΔpH-insensitive NPQ, including state transition- and photoinhibition-dependent quenching (qT and qI, respectively) (Derks et al., 2015), might occur, particularly under high light, in *M. polymorpha*.

### Response of PSII Operating Efficiency to a Submerged Condition in *M. polymorpha*

We measured the responses of Y(II) to a submerged condition in Tak-1, Δ*MpFlv1*, and c*MpFlv1* using an imaging-PAM. *M. polymorpha* thalli on agar were illuminated with blue AL. After photosynthesis reached steady state, we added distilled water to completely submerge the thalli in water. During the transition to a submerged condition, decreases in Y(II) were observed in all three strains, although the change was most prominent in Δ*MpFlv1* (Fig. 7). The diffusion efficiency of $CO_2$ is approximately $10^4$ times lower in aqueous environments compared with in the atmosphere. Submergence limits $CO_2$ supply to Rubisco in chloroplasts. This suppressed photosynthesis would stimulate the FLV-mediated AEF.

## CONCLUSION

We clarified the physiological functions of FLV in the liverwort *M. polymorpha*, which has two genes homologous to *flv1* and *flv3* found in the cyanobacterium S. 6803. In S. 6803, most of the linear electron flow can be passed to FLV1/3 in photosynthesis induction (Helman et al., 2003; Hayashi et al., 2014; Supplemental Fig. S2), and the FLV-mediated AEF partially proceeds at steady-state photosynthesis (Helman et al., 2005). Similar to FLV in S. 6803, the gene product of *MpFlv1* drives AEF in *M. polymorpha*. In the induction phase of photosynthesis, the electron flux mediated by FLV is estimated to contribute to approximately one-quarter of the linear electron flow, at least at the photon flux density we used in this study (Fig. 2), which is smaller than that observed in S. 6803. Nevertheless, FLV-mediated AEF contributes to the oxidation of the PQ pool (Figs. 3C and 5C) and P700 (Figs. 3E and 5E). An absence of *MpFlv1* promotes the photoinhibition of PSI and PSII in *M. polymorpha* (Fig. 1). These results indicate that the physiological roles of FLV have been conserved at the current evolutional stage of basal land plants.

Liverworts probably require FLVs and their functions due to the environmental conditions of their habitats, which is implied by the results in Figure 7. Land plants are exposed to $CO_2$ limitations when submerged, because the diffusion rate of $CO_2$ in the water is much lower than in

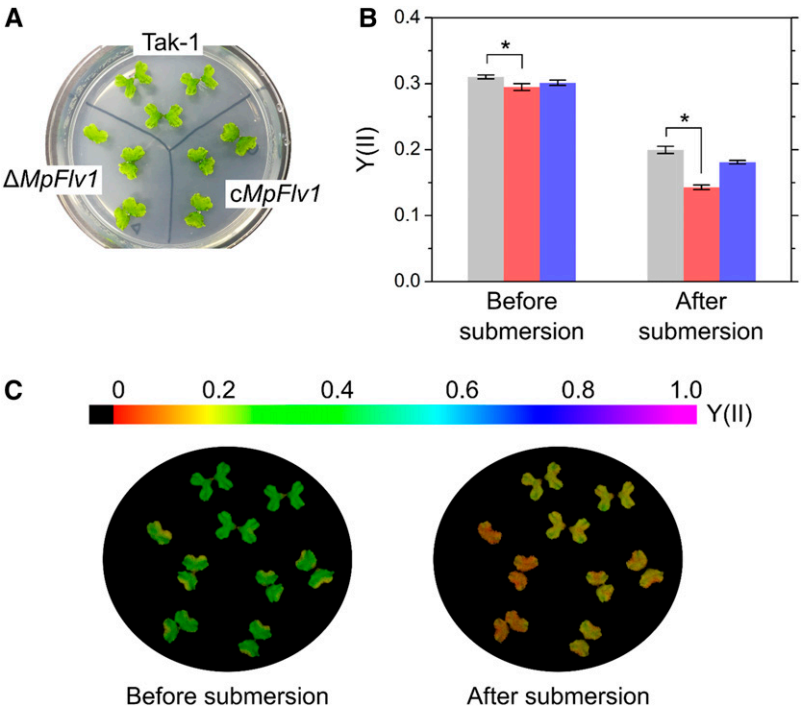


**Figure 7.** Responses of Y(II) to submersion in Tak-1, Δ*MpFlv1*, and c*MpFlv1*. A, Representative images of thalli on an agar medium. B, Y(II) in Tak-1 (light gray bars), Δ*MpFlv1* (pale red bars), and c*MpFlv1* (pale blue bars) before and 20 s after submersion at steady-state photosynthesis. Data are represented as means ± SD of three independent measurements. Differences between Tak-1 and Δ*MpFlv1* were analyzed using Student's *t* test. Asterisks indicate statistically significant differences between Tak-1 and Δ*MpFlv1* at $P < 0.05$. C, Representative fluorescence images of Y(II) before and 20 s after submersion at steady-state photosynthesis. Photon flux density of blue AL was adjusted to 240 $\mu$mol photons $m^{-2}$ $s^{-1}$.

the atmosphere. Generally, in $C_3$ plants exposed to low-$CO_2$ conditions, photorespiration functions as an alternative electron sink to replace photosynthesis (Kozaki and Takeba, 1996; Takahashi et al., 2007), which contributes to the dissipation of excess photon energy and suppresses photooxidative damage. However, in aqueous conditions, the efficiency of ribulose 1,5-bisphosphate oxygenation catalyzed by Rubisco is low, because the affinity of ribulose 1,5-bisphosphate oxygenation reactions for oxygen, $K_m$ for oxygen, ranges from 250 to 450 $\mu$M oxygen (Jordan and Ogren, 1981). The concentration of oxygen in the water equilibrated with the atmosphere is about 250 $\mu$M at 25°C. These facts imply that the photorespiration rate is limited by the supply of oxygen from the atmosphere, and Rubisco cannot turn over at the maximum rate under these conditions. On the other hand, $K_m$ for oxygen in FLV reactions is below a few micromolar oxygen (Vicente et al., 2002; Shimakawa et al., 2015), and FLV catalyzes the reduction of oxygen to water at its maximum rate in the water. In fact, in some species of cyanobacteria (S. 6803, *Synechococcus elongatus* PCC 7942, and *Synechococcus* sp. PCC 7002), under suppressed photosynthesis conditions equilibrated with air, AEF is driven by FLVs, not by photorespiration (Hayashi et al., 2014; Shimakawa et al., 2015, 2016b; Shaku et al., 2016). Furthermore, some eukaryotic algae, including the green alga *Chlamydomonas reinhardtii* and the diatom *Phaeodactylum tricornutum*, do not utilize photorespiration as the main alternative electron sink under suppressed photosynthesis conditions (Shimakawa et al., 2016a, 2017). These facts suggest that oxygenic phototrophs that reside in or are exposed to aqueous environments use FLV in AEF to oxidize P700 in PSI. Recently, the moss *Physcomitrella patens* was reported to show FLV-mediated AEF, similar to *M. polymorpha* (Gerotto et al., 2016). The physiological functions of FLV may be conserved in whole bryophytes.

Here, we propose a model of the mechanisms involved in oxidizing P700 for the suppression of photooxidative damage in PSI derived from ROS in the liverwort *M. polymorpha* (Fig. 8), which appears to be broadly applicable to various oxygenic phototrophs, with the exception of the extent of FLV activity. In angiosperms, which generally do not possess FLV, this mechanism might be replaced with other molecular mechanisms, including the photorespiratory $C_2$ cycle, plastidial terminal oxidase, the Mehler-ascorbate peroxidase pathway, cyclic electron flow (including chloroplast NADPH dehydrogenase and ferredoxin-quinone reductase), and

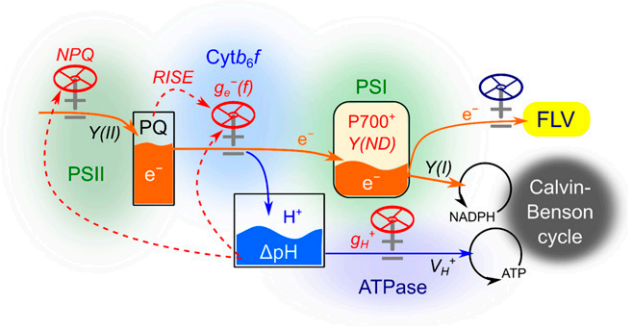


**Figure 8.** Model of the system for P700 oxidation to alleviate photooxidative damage to PSI in *M. polymorpha*. Photosynthetic linear electron flow is indicated by orange arrows. Blue arrows indicate proton flux. Red dashed arrows represent signal pathways regulating flux valves. pmf, Proton motive force. Details are described in the text.

malate dehydrogenase. Additionally, electron transport in the cytochrome $b_6/f$ complex also is suppressed by sensing the redox state of the PQ pool in the reduction-induced suppression of electron flow (RISE) system, which has been characterized in the cyanobacterium *Synechococcus elongatus* PCC 7942 (Shaku et al., 2016) but not yet in photosynthetic eukaryotes. In the RISE system, accumulation of the reduced form of PQ inhibits the Q cycle in cytochrome $b_6/f$. That is, RISE can oxidize P700, where no limitation of the acceptor side of PSI is required as a prerequisite. The physiological functions of RISE in *M. polymorpha* await investigation in future studies. We note that there should be strategic diversity in oxygenic phototrophs commensurate with their survival on the earth.

## MATERIALS AND METHODS

### Culture and Growth Conditions of *Marchantia polymorpha*

A male accession of *M. polymorpha*, Tak-1, was asexually maintained according to previously described methods (Ishizaki et al., 2008). Plants were incubated on one-half-strength Gamborg's B5 agar medium (Gamborg et al., 1968) under a light/dark cycle (14 h of light, 22°C, 100 $\mu$mol photons $m^{-2}$ $s^{-1}$, white fluorescent lamp/10 h of dark, 20°C). For biochemical and physiological measurements of plants, 2-week-old gemmalings were transferred from B5 agar medium onto moist vermiculite.

### Targeted Gene Knockout of *MpFlv1*

To generate the *MpFlv1*-targeting vector, pJHY-TMp1 was used (Ishizaki et al., 2013). The 5′ and 3′ homology arms (4.6 and 4.5 kb, respectively) were amplified from genomic DNA extracted from Tak-1 thalli through PCR using KOD Fx Neo (Toyobo), with the primer sets $T_{up}$ and $T_{dn}$ used for the 5′ and 3′ homology arms, respectively (Supplemental Table S1). The PCR products of these homology arms were cloned into the *Pac*I and *Asc*I sites of pJHY-TMp1 using the In-Fusion HD Cloning Kit (Takara).

Introduction of the targeting construct into *M. polymorpha* was performed using *Rhizobium radiobactor* C58C1 GV2260, as described previously (Ishizaki et al., 2008, 2013). F1 spores generated by crossing Tak-1 and Takaragaike-2 were used for transformation. Isogenic lines (designated as $G_1$ lines) were obtained by isolating gemmae, which develop from single cells, and were screened for gene-targeted lines to use as Δ*MpFlv1* by genotyping using a previously described method (Ishizaki et al., 2013; Supplemental Fig. S1).

### Complementation Lines of Δ*MpFlv1*

To generate complementation lines of Δ*MpFlv1*, a binary vector, pMpGWB306, harboring a mutated acetolactate synthase gene that confers chlorosulfuron resistance was used (Ishizaki et al., 2015). The coding region of *MpFlv1* was amplified from cDNA from Tak-1 through PCR using KOD plus Neo (Toyobo) with the primer set C (Supplemental Table S1) and was then cloned into pENTR/D-TOPO (Thermo Fisher Scientific). The resultant *MpFlv1* cassette was cloned into pMpGWB306 using LR Clonase II (Thermo Fisher Scientific) according to the manufacturer's protocol. The inserted *MpFlv1* was driven by the cauliflower mosaic virus 35S promoter (Ishizaki et al., 2015). Complementation lines were generated by transforming the resulting binary plasmids into regenerating thalli of Δ*MpFlv1*, as described previously (Kubota et al., 2013). Several transformants were obtained through selection with chlorosulfuron and used as c*MpFlv1* lines.

### Measurement of *MpFlv1* Transcripts

Reverse transcription-PCR was performed using KOD Fx Neo (Toyobo) with cDNA from Tak-1, Δ*MpFlv1*, and c*MpFlv1*. We used the *Actin* gene (*Mapoly0016s0137*) as a reference gene. The primer sets used ($RT_{FLV}$ and $RT_{ACT}$) are listed in Supplemental Table S1.

### Measurements of Chl and Nitrogen

The contents of Chl *a* and *b* in the *M. polymorpha* thalli were spectrophotometrically measured using a U-2800A spectrophotometer (Hitachi). For the measurement, extracts of thalli were obtained through incubation in 100% (v/v) *N*,*N*-dimethylformamide overnight. Both the Chl *a* and *b* contents in each extract were determined using the methods of Porra et al. (1989).

To measure nitrogen, *M. polymorpha* thalli were dried overnight at 60°C and then digested via Kjeldahl digestion with sulfuric acid. Total nitrogen contents were determined with Nessler's reagent after adding sodium potassium tartrate (Shimakawa et al., 2014).

### Measurements of Oxygen Exchange and Chl Fluorescence

Oxygen exchange was monitored simultaneously with Chl fluorescence. Thalli (2−5 $cm^2$) were set in the oxygen electrode chamber (LD2/3; Hansatech), and Chl fluorescence was monitored using a Junior-PAM Chl fluorometer (Walz) through a light-guided plastic-fiber set into the oxygen electrode chamber (Sejima et al., 2016). The temperature of the chamber was set to 25°C. Red AL was illuminated from the top of the oxygen electrode chamber, and the photon flux densities were adjusted to the values indicated in the corresponding figure legends. Since the oxygen electrode chamber was a closed system, $CO_2$-saturated conditions were simulated by placing a fabric mat wetted with 1 M $NaHCO_3$ solution below the intact thalli to supply $CO_2$ at a concentration of approximately 1% (v/v). The photosynthetic parameters in PSII were calculated using Chl fluorescence parameters as described below (see "Measurements of Chl Fluorescence and P700").

For the measurements of oxygen exchange and Chl fluorescence in the liquid phase, we used an oxygen electrode chamber (DW2/2; Hansatech), a PAM-101 Chl fluorometer (Walz), and cyanobacterial cells grown under high-$CO_2$ conditions according to the methods of Shimakawa et al. (2016a). The reaction mixture (2 mL) contained 50 mM HEPES (pH 7.5), 10 mM $NaHCO_3$, and the cyanobacterial cells (10 $\mu$g Chl $mL^{-1}$). Cells were illuminated with red AL ($620 < \lambda < 695$ nm, 240 $\mu$mol photons $m^{-2}$ $s^{-1}$) at 25°C. During the measurements, the reaction mixture was stirred with a magnetic microstirrer. Pulse-modulated excitation was achieved using a light-emitting diode lamp with a peak emission of 650 nm. Modulated fluorescence was measured at $\lambda > 710$ nm (Schott RG9 long-pass filter). The photosynthetic parameters in PSII were calculated using Chl fluorescence parameters, as described below (see "Measurements of Chl Fluorescence and P700").

### Measurements of Chl Fluorescence and P700

Both Chl fluorescence and $P700^+$ were measured simultaneously using a Dual-PAM-100 fluorometer (Walz). In this measurement, we used a 3010 DUAL gas-exchange leaf chamber (Walz). Ambient air was saturated with water vapor at 18°C ± 0.1°C, and the leaf temperature was maintained at 25°C. The photosynthetic parameters in PSII were calculated using Chl fluorescence parameters as follows (Baker, 2008): $F_v/F_m = (F_m - F_o)/F_m$, $Y(II) = (F_m' - F')/F_m'$, $NPQ = (F_m - F_m')/F_m'$, and $qP = (F_m' - F')/(F_m' - F_o)$, where $F_o$, minimum fluorescence from a dark-adapted leaf; $F_m$, maximum fluorescence from a dark-adapted leaf; $F_m'$, maximum fluorescence from a light-adapted leaf; and $F'$, fluorescence emission from a light-adapted leaf. Pulse amplitude-modulated measuring light (0.1 $\mu$mol photons $m^{-2}$ $s^{-1}$) was applied to determine $F_o$. Short-saturation pulses (10,000 $\mu$mol photons $m^{-2}$ $s^{-1}$, 300 ms) were applied to determine $F_m$ and $F_m'$.

The photosynthetic parameters in PSI were calculated from the redox state of P700 as follows (Klughammer and Schreiber, 1994; Schreiber and Klughammer, 2008): $Y(I) = (P_m' - P)/P_m$, $Y(NA) = (P_m - P_m')/P_m$, and $Y(ND) = P/P_m$, where $P_m$, total amount of photooxidizable P700; $P_m'$, maximum amount of photooxidized P700 by a saturation pulse; and $P$, amount of photooxidized P700 at steady state. Red AL was used to measure the photosynthetic parameters at photon flux densities, as indicated in the corresponding figure legends.

For measurements in the absence of oxygen, pure $N_2$ gas was prepared and saturated with water vapor at 18°C ± 0.1°C.

During analysis with an Imaging-PAM (M-Series; Walz), pulse-modulated excitation, actinic illumination, and saturation pulses were achieved with a blue light-emitting diode lamp with a peak emission of 450 nm. Images of the fluorescence parameters were displayed with the help of a false-color code ranging from black (0) through red, yellow, green, blue, and pink (1; Singh et al., 2013).

### Measurement of ECS

ECS was measured using a Dual-PAM-100 fluorometer equipped with a P515-analysis module (Klughammer et al., 2013). In this measurement, we used a

3010 DUAL gas-exchange leaf chamber (Walz). Ambient air was saturated with water vapor at 18°C ± 0.1°C, and the leaf temperature was maintained at 25°C. ECSt, $g_H^+$ in ATP synthase, and $V_H^+$ were measured through DIRK analysis, as described by Sacksteder and Kramer (2000) and Baker et al. (2007). For the DIRK analysis, we set the transient dark (600 ms) during illumination with AL. We measured the extent of the change in ECS as ECSt and the half-life of ECS decay for the calculation of $g_H^+(s^{-1})$. During the transient dark, $V_H^+$ was estimated from the initial decay of ECS. The values of ECSt were normalized by dividing the magnitude of ECS decay in DIRK analysis by the magnitude of ECS induced by a 10-$\mu$s single-turnover flash (Klughammer et al., 2013). In separate experiments, ECSt was divided into ΔpH and ΔΨ following the methods of Klughammer et al. (2013).

## Statistical Analysis

We used Student's *t* test to detect differences. All statistical analyses were performed using Microsoft Excel 2010 (Microsoft) and JMP8 (SAS Institute).

## Accession Numbers

The sequence data used in this study are originated from a preliminary genome database.

## Supplemental Data

The following supplemental materials are available.

**Supplemental Figure S1.** Strategy for targeted disruption of the *MpFlv1* locus and analysis of homologous recombination events.

**Supplemental Figure S2.** Time course of gross photosynthetic oxygen evolution rates and Y(II) in the induction phase of photosynthesis in S. 6803 wild type and Δ*flv1/3*.

**Supplemental Figure S3.** Dependence of gross photosynthetic oxygen evolution rates and Y(II) on photon flux density at steady-state photosynthesis in Tak-1, Δ*MpFlv1*, and c*MpFlv1*.

**Supplemental Figure S4.** Representative original traces of dark-interval relaxation kinetics of ECS in Tak-1 and Δ*MpFlv1*.

**Supplemental Figure S5.** Time course of ECSt, $g_H^+$, and $V_H^+$ in the transition from moderate to high light in Tak-1, Δ*MpFlv1*, and c*MpFlv1*.

**Supplemental Figure S6.** Dependence of rETR, ECSt, $g_H^+$, and $V_H^+$ on photon flux density at steady-state photosynthesis in Tak-1, Δ*MpFlv1*, and c*MpFlv1*.

**Supplemental Figure S7.** Dependence of ECSt, ΔpH, and ΔΨ on photon flux density and the relationship of ECSt, ΔpH, and ΔΨ to the rETR at steady-state photosynthesis in Tak-1, Δ*MpFlv1*, and c*MpFlv1*.

**Supplemental Figure S8.** Relationship of NPQ to the rETR at steady-state photosynthesis in Tak-1, Δ*MpFlv1*, and c*MpFlv1*.

**Supplemental Figure S9.** Relaxation of NPQ after transition to the dark.

**Supplemental Table S1.** Primers used in this study.

Received July 5, 2016; accepted January 31, 2017; published February 2, 2017.

## LITERATURE CITED

**Allahverdiyeva Y, Mustila H, Ermakova M, Bersanini L, Richaud P, Ajlani G, Battchikova N, Cournac L, Aro EM** (2013) Flavodiiron proteins Flv1 and Flv3 enable cyanobacterial growth and photosynthesis under fluctuating light. Proc Natl Acad Sci USA **110:** 4111–4116

**Asada K** (1999) The water-water cycle in chloroplasts: scavenging of active oxygens and dissipation of excess photons. Annu Rev Plant Physiol Plant Mol Biol **50:** 601–639

**Avenson TJ, Cruz JA, Kanazawa A, Kramer DM** (2005) Regulating the proton budget of higher plant photosynthesis. Proc Natl Acad Sci USA **102:** 9709–9713

**Avenson TJ, Cruz JA, Kramer DM** (2004) Modulation of energy-dependent quenching of excitons in antennae of higher plants. Proc Natl Acad Sci USA **101:** 5530–5535

**Badger MR, Spalding MH** (2000) $CO_2$ acquisition, concentration and fixation in cyanobacteria and algae. *In* RC Leegood, TD Sharkey, S von Caemmerer, eds, Photosynthesis: Physiology and Metabolism. Springer, Dordrecht, The Netherlands, pp 369–397

**Bailleul B, Cardol P, Breyton C, Finazzi G** (2010) Electrochromism: a useful probe to study algal photosynthesis. Photosynth Res **106:** 179–189

**Baker NR** (2008) Chlorophyll fluorescence: a probe of photosynthesis in vivo. Annu Rev Plant Biol **59:** 89–113

**Baker NR, Harbinson J, Kramer DM** (2007) Determining the limitations and regulation of photosynthetic energy transduction in leaves. Plant Cell Environ **30:** 1107–1125

**Boardman NK** (1977) Comparative photosynthesis of sun and shade plants. Annu Rev Plant Physiol **28:** 355–377

**Bowman JL, Floyd SK, Sakakibara K** (2007) Green genes: comparative genomics of the green branch of life. Cell **129:** 229–234

**Cazzaniga S, Li Z, Niyogi KK, Bassi R, Dall'Osto L** (2012) The Arabidopsis *szl1* mutant reveals a critical role of $\beta$-carotene in photosystem I photoprotection. Plant Physiol **159:** 1745–1758

**Cruz JA, Kanazawa A, Treff N, Kramer DM** (2005) Storage of light-driven transthylakoid proton motive force as an electric field ($\Delta\psi$) under steady-state conditions in intact cells of Chlamydomonas reinhardtii. Photosynth Res **85:** 221–233

**Cruz JA, Sacksteder CA, Kanazawa A, Kramer DM** (2001) Contribution of electric field ($\Delta\ \psi$) to steady-state transthylakoid proton motive force (*pmf*) in vitro and in vivo: control of *pmf* parsing into $\Delta\ \psi$ and $\Delta$ pH by ionic strength. Biochemistry **40:** 1226–1237

**Derks A, Schaven K, Bruce D** (2015) Diverse mechanisms for photoprotection in photosynthesis: dynamic regulation of photosystem II excitation in response to rapid environmental change. Biochim Biophys Acta **1847:** 468–485

**Fischer BB, Hideg É, Krieger-Liszkay A** (2013) Production, detection, and signaling of singlet oxygen in photosynthetic organisms. Antioxid Redox Signal **18:** 2145–2162

**Gamborg OL, Miller RA, Ojima K** (1968) Nutrient requirements of suspension cultures of soybean root cells. Exp Cell Res **50:** 151–158

**Gerotto C, Alboresi A, Meneghesso A, Jokel M, Suorsa M, Aro EM, Morosinotto T** (2016) Flavodiiron proteins act as safety valve for electrons in *Physcomitrella patens*. Proc Natl Acad Sci USA **113:** 12322–12327

**Hayashi R, Shimakawa G, Shaku K, Shimizu S, Akimoto S, Yamamoto H, Amako K, Sugimoto T, Tamoi M, Makino A, et al** (2014) $O_2$-dependent large electron flow functioned as an electron sink, replacing the steady-state electron flux in photosynthesis in the cyanobacterium *Synechocystis* sp. PCC 6803, but not in the cyanobacterium *Synechococcus* sp. PCC 7942. Biosci Biotechnol Biochem **78:** 384–393

**Helman Y, Barkan E, Eisenstadt D, Luz B, Kaplan A** (2005) Fractionation of the three stable oxygen isotopes by oxygen-producing and oxygen-consuming reactions in photosynthetic organisms. Plant Physiol **138:** 2292–2298

**Helman Y, Tchernov D, Reinhold L, Shibata M, Ogawa T, Schwarz R, Ohad I, Kaplan A** (2003) Genes encoding A-type flavoproteins are essential for photoreduction of $O_2$ in cyanobacteria. Curr Biol **13:** 230–235

**Ishizaki K, Chiyoda S, Yamato KT, Kohchi T** (2008) *Agrobacterium*-mediated transformation of the haploid liverwort *Marchantia polymorpha* L., an emerging model for plant biology. Plant Cell Physiol **49:** 1084–1091

**Ishizaki K, Johzuka-Hisatomi Y, Ishida S, Iida S, Kohchi T** (2013) Homologous recombination-mediated gene targeting in the liverwort *Marchantia polymorpha* L. Sci Rep **3:** 1532

**Ishizaki K, Nishihama R, Ueda M, Inoue K, Ishida S, Nishimura Y, Shikanai T, Kohchi T** (2015) Development of Gateway binary vector series with four different selection markers for the liverwort *Marchantia polymorpha*. PLoS ONE **10:** e0138876

**Johnson MP, Ruban AV** (2014) Rethinking the existence of a steady-state $\Delta\psi$ component of the proton motive force across plant thylakoid membranes. Photosynth Res **119:** 233–242

**Jordan DB, Ogren WL** (1981) Species variation in the specificity of ribulose bisphosphate carboxylase/oxygenase. Nature **291:** 513–515

**Kanazawa A, Kramer DM** (2002) *In vivo* modulation of nonphotochemical exciton quenching (NPQ) by regulation of the chloroplast ATP synthase. Proc Natl Acad Sci USA **99:** 12789–12794

**Klughammer C, Schreiber U** (1994) An improved method, using saturating light pulses, for the determination of photosystem I quantum yield via $P700^+$-absorbance changes at 830 nm. Planta **192:** 261–268

**Klughammer C, Siebke K, Schreiber U** (2013) Continuous ECS-indicated recording of the proton-motive charge flux in leaves. Photosynth Res **117:** 471–487

**Kozaki A, Takeba G** (1996) Photorespiration protects C3 plants from photooxidation. Nature **384:** 557–560

**Kramer DM, Sacksteder CA, Cruz JA** (1999) How acidic is the lumen? Photosynth Res **60:** 151–163

**Krause GH, Köster S, Wong SC** (1985) Photoinhibition of photosynthesis under anaerobic conditions studied with leaves and chloroplasts of *Spinacia oleracea* L. Planta **165:** 430–438

**Krieger-Liszkay A** (2005) Singlet oxygen production in photosynthesis. J Exp Bot **56:** 337–346

**Kubota A, Ishizaki K, Hosaka M, Kohchi T** (2013) Efficient *Agrobacterium*-mediated transformation of the liverwort *Marchantia polymorpha* using regenerating thalli. Biosci Biotechnol Biochem **77:** 167–172

**Laisk A, Eichelmann H, Oja V, Rasulov B, Rämma H** (2006) Photosystem II cycle and alternative electron flow in leaves. Plant Cell Physiol **47:** 972–983

**Miyake C** (2008) Coupled regulation of cyclic electron flow around PSI with photosynthesis: its contribution to non-photochemical quenching evidenced with transplastomic tobacco plants over-expressing ferredoxin in chloroplasts. *In* JF Allen, E Gantt, JH Golbeck, B Osmond, eds, Photosynthesis: Energy from the Sun. 14th International Congress on Photosynthesis. Springer, Dordrecht, The Netherlands, pp 923–927

**Miyake C** (2010) Alternative electron flows (water-water cycle and cyclic electron flow around PSI) in photosynthesis: molecular mechanisms and physiological functions. Plant Cell Physiol **51:** 1951–1963

**Miyake C, Okamura M** (2003) Cyclic electron flow within PSII protects PSII from its photoinhibition in thylakoid membranes from spinach chloroplasts. Plant Cell Physiol **44:** 457–462

**Miyake C, Yokota A** (2001) Cyclic flow of electrons within PSII in thylakoid membranes. Plant Cell Physiol **42:** 508–515

**Miyake C, Yonekura K, Kobayashi Y, Yokota A** (2002) Cyclic electron flow within PSII functions in intact chloroplasts from spinach leaves. Plant Cell Physiol **43:** 951–957

**Porra R, Thompson W, Kriedelman P** (1989) Determination of accurate extraction and simultaneously equation for assaying chlorophyll *a* and *b* extracted with different solvents: verification of the concentration of chlorophyll standards by atomic absorption spectroscopy. Biochim Biophys Acta **975:** 384–394

**Raven JA, Osborne BA, Johnston AM** (1985) Uptake of $CO_2$ by aquatic vegetation. Plant Cell Environ **8:** 417–425

**Rutherford AW, Osyczka A, Rappaport F** (2012) Back-reactions, short-circuits, leaks and other energy wasteful reactions in biological electron transfer: redox tuning to survive life in $O_2$. FEBS Lett **586:** 603–616

**Sacksteder CA, Kramer DM** (2000) Dark-interval relaxation kinetics (DIRK) of absorbance changes as a quantitative probe of steady-state electron transfer. Photosynth Res **66:** 145–158

**Schreiber U, Klughammer C** (2008) Saturation pulse method for assessment of energy conversion in PSI. PAM Appl Notes **1:** 11–14

**Sejima T, Hanawa H, Shimakawa G, Takagi D, Suzuki Y, Fukayama H, Makino A, Miyake C** (2016) Post-illumination transient $O_2$-uptake is driven by photorespiration in tobacco leaves. Physiol Plant **156:** 227–238

**Sejima T, Takagi D, Fukayama H, Makino A, Miyake C** (2014) Repetitive short-pulse light mainly inactivates photosystem I in sunflower leaves. Plant Cell Physiol **55:** 1184–1193

**Shaku K, Shimakawa G, Hashiguchi M, Miyake C** (2016) Reduction-induced suppression of electron flow (RISE) in the photosynthetic electron transport system of *Synechococcus elongatus* PCC 7942. Plant Cell Physiol **57:** 1443–1453

**Shimakawa G, Akimoto S, Ueno Y, Wada A, Shaku K, Takahashi Y, Miyake C** (2016a) Diversity in photosynthetic electron transport under $[CO_2]$-limitation: the cyanobacterium *Synechococcus* sp. PCC 7002 and green alga *Chlamydomonas reinhardtii* drive an $O_2$-dependent alternative electron flow and non-photochemical quenching of chlorophyll fluorescence during $CO_2$-limited photosynthesis. Photosynth Res **130:** 293–305

**Shimakawa G, Hasunuma T, Kondo A, Matsuda M, Makino A, Miyake C** (2014) Respiration accumulates Calvin cycle intermediates for the rapid start of photosynthesis in *Synechocystis* sp. PCC 6803. Biosci Biotechnol Biochem **78:** 1997–2007

**Shimakawa G, Matsuda Y, Nakajima K, Tamoi M, Shigeoka S, Miyake C** (2017) Diverse strategies of $O_2$ usage for preventing photo-oxidative damage under $CO_2$ limitation during algal photosynthesis. Sci Rep **7:** 41022

**Shimakawa G, Shaku K, Miyake C** (2016b) Oxidation of P700 in photosystem I is essential for the growth of cyanobacteria. Plant Physiol **172:** 1443–1450

**Shimakawa G, Shaku K, Nishi A, Hayashi R, Yamamoto H, Sakamoto K, Makino A, Miyake C** (2015) FLAVODIIRON2 and FLAVODIIRON4 proteins mediate an oxygen-dependent alternative electron flow in *Synechocystis* sp. PCC 6803 under $CO_2$-limited conditions. Plant Physiol **167:** 472–480

**Singh R, Ranjan S, Nayaka S, Pathre UV, Shirke PA** (2013) Functional characteristics of a fruticose type of lichen, *Stereocaulon foliolosum* Nyl. in response to light and water stress. Acta Physiol Plant **35:** 1605–1615

**Takagi D, Takumi S, Hashiguchi M, Sejima T, Miyake C** (2016) Superoxide and singlet oxygen produced within the thylakoid membranes both cause photosystem I photoinhibition. Plant Physiol **171:** 1626–1634

**Takahashi S, Bauwe H, Badger M** (2007) Impairment of the photorespiratory pathway accelerates photoinhibition of photosystem II by suppression of repair but not acceleration of damage processes in Arabidopsis. Plant Physiol **144:** 487–494

**Takizawa K, Cruz JA, Kanazawa A, Kramer DM** (2007) The thylakoid proton motive force *in vivo*: quantitative, non-invasive probes, energetics, and regulatory consequences of light-induced *pmf*. Biochim Biophys Acta **1767:** 1233–1244

**Vicente JB, Gomes CM, Wasserfallen A, Teixeira M** (2002) Module fusion in an A-type flavoprotein from the cyanobacterium *Synechocystis* condenses a multiple-component pathway in a single polypeptide chain. Biochem Biophys Res Commun **294:** 82–87

**Witt HT** (1979) Energy conversion in the functional membrane of photosynthesis: analysis by light pulse and electric pulse methods. The central role of the electric field. Biochim Biophys Acta **505:** 355–427

**Yamamoto H, Takahashi S, Badger MR, Shikanai T** (2016) Artificial remodelling of alternative electron flow by flavodiiron proteins in Arabidopsis. Nat Plants **2:** 16012

**Zhang P, Eisenhut M, Brandt AM, Carmel D, Silén HM, Vass I, Allahverdiyeva Y, Salminen TA, Aro EM** (2012) Operon *flv4-flv2* provides cyanobacterial photosystem II with flexibility of electron transfer. Plant Cell **24:** 1952–1971

**Zivcak M, Brestic M, Kunderlikova K, Olsovska K, Allakhverdiev SI** (2015a) Effect of photosystem I inactivation on chlorophyll *a* fluorescence induction in wheat leaves: does activity of photosystem I play any role in OJIP rise? J Photochem Photobiol B **152:** 318–324

**Zivcak M, Brestic M, Kunderlikova K, Sytar O, Allakhverdiev SI** (2015b) Repetitive light pulse-induced photoinhibition of photosystem I severely affects $CO_2$ assimilation and photoprotection in wheat leaves. Photosynth Res **126:** 449–463